Development of Fe/TiO$_2$ Photocatalyst for Hydrogen Production from Water under Visible Light

by

Noor Herniza Binti Basar

Dissertation submitted in partial fulfilment of

the requirements for the

Bachelor of Engineering (Hons)

(Chemical Engineering)

July 2010

Universiti Teknologi PETRONAS
Bandar Seri Iskandar
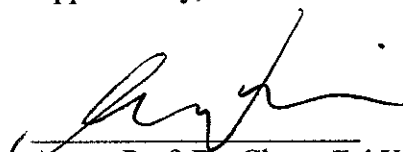31750 Tronoh
Perak Darul Ridzuan

CERTIFICATION OF APPROVAL

Development of Fe/TiO$_2$ Photocatalyst for Hydrogen Production from Water under Visible Light

by

Noor Herniza Binti Basar

A project dissertation submitted to the

Chemical Engineering Programme

Universiti Teknologi PETRONAS

in partial fulfilment of the requirement for the

BACHELOR OF ENGINEERING (Hons)

(CHEMICAL ENGINEERING)

Approved by,

_____ 15/12/10

Assoc. Prof. Dr. Chong Fai Kait

Project Supervisor

Assoc. Prof. Dr. Chong Fai Kait
Fundamental and Applied Sciences Department
Universiti Teknologi PETRONAS
Bandar Seri Iskandar, 31750 Tronoh
Perak Darul Ridzuan, MALAYSIA

UNIVERSITI TEKNOLOGI PETRONAS

TRONOH, PERAK

January 2006

CERTIFICATION OF ORIGINALITY

This is to certify that I am responsible for the work submitted in this project, that the original work is my own except as specified in the references and acknowledgements, and that the original work contained herein have not been undertaken or done by unspecified sources or persons.

NOOR HERNIZA BINTI BASAR

ABSTRACT

Solar energy is concerned in order to generate hydrogen (H_2) from water with the present of photocatalyst. The main problem is that current titanium dioxide (TiO_2) photocatalyst is only active in the ultraviolet (UV) region. In order to harvest the abundance solar radiation consisting mainly of visible light, the efficiency of TiO_2 has to be increased by shifted the absorption edge of TiO_2 to the visible region. In order to increase the efficiency, the TiO_2 photocatalyst is modified via metal doping method. The production of hydrogen over iron-doped titanium dioxide (Fe/TiO_2) photocatalyst prepared by precipitation method has been studied. The iron (Fe) loading varied from 0.1 to 1.0 wt% with different calcination temperature at $300°C$, $400°C$ and $500°C$. The photocatalyst was characterized by Thermogravimetric Analysis (TGA), Diffuse Reflectance UV-Vis (DR UV-Vis), Fourier Transform Infrared (FTIR) Spectroscopy, X-ray Diffraction (XRD), and Field Emission Scanning Electron Microscopy (FE-SEM). The UV–vis absorption spectrum indicated that the absorption edge of the photocatalyst red-shifted to around 600 nm. The lowest reduction of band gap as a result of Fe doping was obtained at 1.0wt% Fe/TiO_2 calcined at $500°C$ (3.08 eV) compared to pure TiO_2 (3.20 eV). Photocatalytic activity towards H_2 generation from water was investigated using a multiport photocatalytic reactor by using halogen lamp that represented solar radiation. Under the irradiation with ultraviolet and visible light, the photocatalyst showed good performance for H_2 production at 1,0 wt% of Fe loading calcined at $500°C$ with the production rate of 6.9 mL. The other characterizations of the photocatalyst were explained throughout this report.

ACKNOWLEDGEMENT

First and foremost, highest thanks to The Almighty, the source of life, wisdom and hope for giving the author the strength and patience to pursue and complete this Final Year Project in blue colours.

The author's utmost gratitude goes to the author's supervisor, Dr. Chong Fai Kait for the informative supervision and valuable knowledge throughout the project. Without her guidance and patience, the author would not be succeeded to complete the project. Thank you to the Final Year Research Project Coordinator, Dr. Khalik and Dr. Mohanad for providing her with all the initial information required to begin the project.

The author's sincere thanks to Chemical Engineering Department of Universiti Teknologi PETRONAS (UTP) for providing this chance to undertake this remarkable final year project. Special thanks also to Ms. Ela for her kind cooperation and assistance in tutoring the author throughout the project. For the entire lab technologies in Chemical Engineering, Civil Engineering and Mechanical Engineering Department, thank you for assisting the author in completing her project.

Last but not least, special credit goes to the author's parents, family members and friends, who had dedicatedly provided the author with additional support and encouragement throughout this project either directly or indirectly. Thanks again to all, your kindness and helps will always be remembered.

TABLE OF CONTENT

LIST OF ILLUSTRATION

List of Figures

List of Tables

Abbreviations and Nomenclatures

CB	Conduction Band
CdS	Cadmium sulfide
CeO_2	Cerium (IV) oxide
Cr	Cromium
Cu	Copper
DR UV-Vis	Diffuse Reflectance UV-Vis
EDX	Energy Dispersive X-ray
Fe	Iron
Fe (acac)$_3$	Iron (III) acetylacetonate
FeO	Iron oxide
$Fe(NO_3)_3$	Iron (III) nitrate
Fe $(NO_3)_3 \cdot 9H_2O$	Iron (III) nitrate nanohydrate
FESEM	Field Emission Scanning Electron Microscopy
Fe/TiO_2	Iron-doped titanium dioxide
FTIR	Fourier Transform Infrared Spectroscopy
H_2	Hydrogen
H-O-H	Hydrogen-Oxygen-Hydrogen bonding
Mn	Manganese

Ni	Nickel
NO_3^-	Nitrate
O-H	Oxygen-Hydrogen bonding
RF-magnetron	Radio Frequency-magnetron
TGA	Thermogravimetric Analysis
$TiCl_4$	Titanium tetrachloride
TiO_2	Titanium dioxide, Titania
UV	Ultraviolet
VB	Valence Band
XRD	X-ray Diffraction
Zn	Zinc
ZnO	Zinc oxide
ZrO_2	Zirconium dioxide

CHAPTER 1

INTRODUCTION

1.1 Background of Study

Energy source for the future is one of the most important global issues because of the nearly depletion. Furthermore, the current energy sources such as fossil fuels give the gross effect to the environment. Due to that, hydrogen is found to be an attractive candidate for the energy carrier of the future (Dholam *et al.*, 2009).

1.1.1 Hydrogen, H_2

Hydrogen Production Processes

Hydrogen bound to organic matter and in water makes up 70% of the earth's surface. Breaking up these bonds in water allows us to produce hydrogen and then to use it as an energy carrier. There are numerous processes that can be used to break these bonds. Below are few methods for producing hydrogen that are currently used, or are under research and development.

- Steam reforming
- Electrolysis
- Steam Electrolysis
- Thermochemical water splitting
- Photoelectrochemical processes
- Biological and photobiological processes

1.1.2 Photocatalyst

Semiconductor catalysts of the chalcogenide type consist of oxides (e.g. TiO_2, ZnO, ZrO_2, CeO_2) or sulfides (CdS, Zn). The most commonly used as photocatalyst is Titanium dioxide, TiO_2 that also known as Titania. Areas of activity in TiO_2 photocatalysis include:

Fog Proof and Self Cleaning Glass

Generally if moist air comes in contact with glass, small droplets of water are formed, and the glass becomes fogged. On TiO_2 coated glass, the water forms a continuous flat sheet, so that there is no fogging.

Anti-Bacterial, Anti-Viral, Fungicidal

Tiles in a hospital are coated with TiO_2 to reduce the bacteria on the wall.

Anti-Soiling, Self Cleaning

TiO_2 can be coated on many building materials. These films exhibit a self cleaning effect due to the strong oxidizing properties.

Water Treatment, Water Purification

Water treatment appears as the most promising potential application since many toxic water pollutants, either organic or inorganic, are totally mineralized or oxidized at their higher degree, respectively, into harmless final compounds.
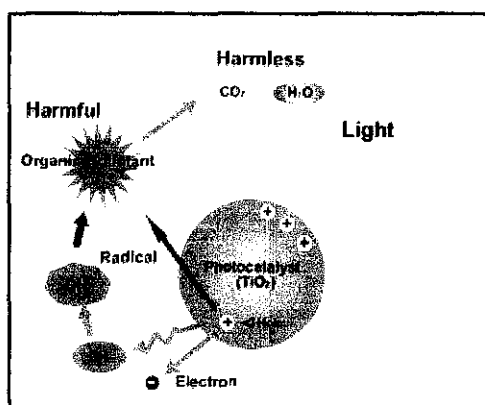
Figure 1.1: Mechanism of Photocatalysis

2

Hydrogen Production from Water

TiO_2 is the most preferred material as a photocatalyst in hydrogen production because of the following properties:

- high resistance to corrosion and photocorrosion in aqueous media
- cheap and easy availability
- environmental friendliness
- energy band edges which are well-matched with the redox level of water
- electronic properties that can be varied by just changing the lattice defect chemistry or the oxygen stoichiometry (Dholam *et al.*, 2009)

In the industry, TiO_2 also can be found in all kinds of paint, printing ink, plastics, paper, synthetic fibers, rubber, condensers, painting colors and crayons, ceramics, electronic components along with food and cosmetics.

1.2   Problem Statement

The sun gives energy of 3×10^{24} joules/year to the earth which is 10,000 times of our current global energy consumption. Furthermore, the world is blessed with a vast abundance of desert lands (19.2×10^6 km^2) (Craig, 2008) that, if we can imagine, it would be ideally suitable for capturing solar energy in a sustainable fashion for the use of society. Solar energy can be used to generate hydrogen from water in the presence of photocatalyst. Current TiO_2 photocatalyst is active only in the UV region. In order to take advantage of the abundant solar radiation consisting mainly of visible light, the absorption edge of TiO_2 has to be shifted to the visible region.

1.3   Objective and Scope of Study

The objective of this study is to develop Fe/TiO_2 photocatalyst for hydrogen production from water in the visible light.

The scope of study involves preparation of Fe/TiO_2 photocatalyst using precipitation method with different Fe loading and pretreatment conditions. The catalyst will be characterized using FE-SEM, XRD, DR UV-Vis, FTIR, and TGA. This study also involves the activity performance of the photocatalyst for H_2 generation from water.

1.4   The Relevancy of The Project

World nowadays starts to realize about the depleting source of energy and try to find alternatives for the energy sources (coal, oil, gas). This project evaluates one of the alternatives for the production of hydrogen from water, thus it is a meaningful project for sustainable development.

CHAPTER 2

LITERATURE REVIEW

2.1   Titanium Dioxide/Titania (TiO₂) Photocatalyst with Metal Doped

Titanium dioxide (TiO_2) is an active photocatalyst under ultraviolet (UV) light with a band gap of 3.2 eV.

$$E = h\nu = \frac{hc}{\lambda}$$
(2.1)

Where:

E= a band gap energy (for TiO_2= 3.2 eV = $3.2 \times 1.6 \times 10^{-19}$ J)

h= Plank's constant (6.63×10^{-34} J.s)

ν= frequency of light (s^{-1})

c= light speed (3.0×10^{8} m/s)

λ= wavelength

Calculation using equation 2.1 shows that the necessary wavelength is approximate 380 nm which represents the UV region.
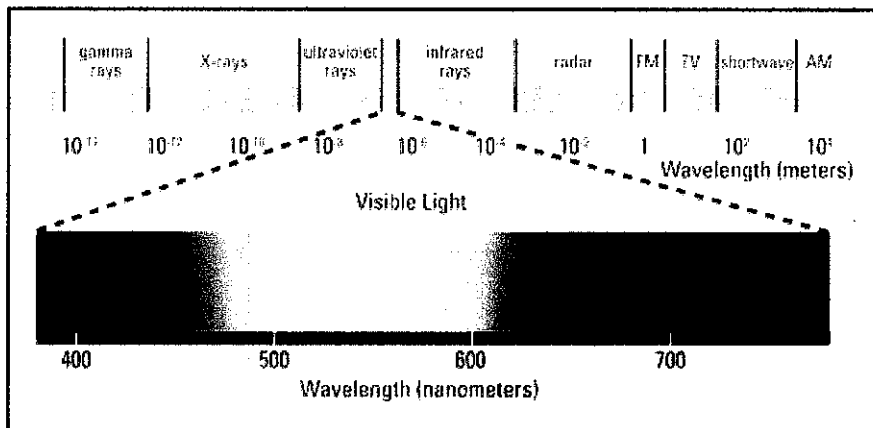

Figure 2.1: Electromagnetic Spectrum

When titanium dioxide (TiO$_2$) absorbs ultraviolet (UV) radiation from sunlight or light source (fluorescent lamps), it will be excited to a high-energy state and releases electrons from its illuminated surface. If the energy received at this stage is high enough, electrons that were initially located in the so-called 'valence band' (VB) will transfer to the 'conduction band' (CB) therefore creating the negative-electron (e-) and positive-hole (h+) pair. The energy difference between VB and CB is known as the 'Band Gap'.

$$TiO_2 + h\nu \rightarrow e^-_{CB} + h^+_{VB}$$
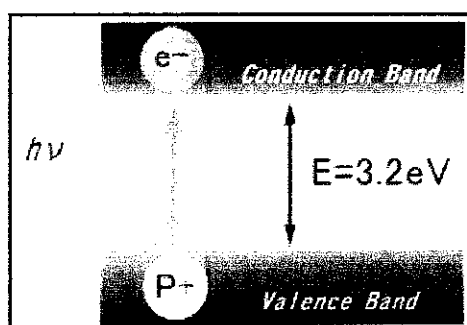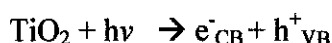
Figure 2.2: Band gap

As discussed above, TiO$_2$ is the most preferred material as a photocatalyst in hydrogen production because some of its advantages. However, TiO$_2$ is active only under ultraviolet (UV) light. Only a small UV fraction of 2-3% of solar light that reaches the earth can be utilized (Kitano *et al.*, 2008). Thus, TiO$_2$ photocatalyst cannot efficiently exploit the abundant natural resource, *i.e.* solar radiation dominantly consists of visible light. It is a great important of TiO$_2$ sensitization to react to the much larger visible regions. Thus, for efficient photocatalytic activity it is necessary to extend the photo-response of TiO$_2$ to the visible spectrum by modification of its optical properties. Another problem is the high recombination rate of photo-generated electron–hole pairs which can be limited by introducing charge traps for electrons and/or holes, thus prolonging the recombination time (Dholam *et al.*, 2009).

Many methods have been proposed to solve these problems, but doping TiO_2 with metal ions is one of the most promising strategies for sensitizing TiO_2 to visible light that introduce additional energy levels in the band gap of TiO_2. It also forms charge traps to keep electron–hole pairs separated (Fujishima *et al.*, 2008). Among these transition metals, Fe, Cu, and Mn are able to trap both electrons and holes, while Cr and Ni are capable of trapping only single charge carriers (Litter *et al.*, 1996). Thus, doping with the former metal ions is better for enhancing photocatalytic activity than with the latter ones.

Charge transfer is an important consideration for photocatalytic reaction. There exists an optimum concentration of dopant metal ions above which the photo- catalytic activity decreases because of charge recombination (Dholam *et al.*, 2009). Yoong *et al.* (2009) reported on hydrogen production under visible light irradiation using Cu-doped TiO_2. The authors clearly showed an increase in H_2 production rate with the concentration of Cu up to a certain optimum value. The result of hydrogen production for 10% of Cu-doped TiO_2 was higher than 15% concentration, 8.4 and 4.6 mL/h, respectively. It shows that metal-doped TiO_2 used for photocatalytic enhanced the activity only for a specific amount of doping ions, otherwise will cause detrimental effects.

2.2   Mechanism of Fe-doped TiO$_2$ Photocatalyst
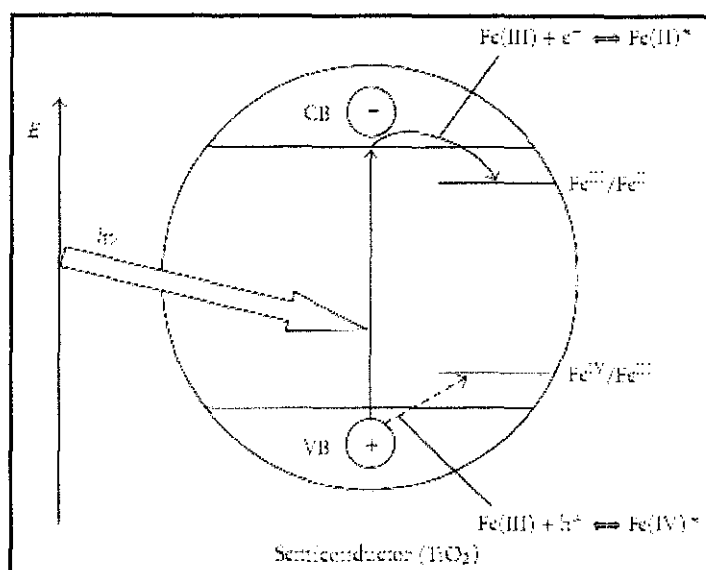
Figure 2.3: Scheme of mechanism of TiO2 photocatalysis with
modification by Fe (III) ion doping

It is generally accepted that Fe (III) centre form shallow charge trapping sites within the TiO$_2$ matrix as well as on the particle surface through the replacement of Ti (IV) by Fe (III) (Litter *et al.*, 1996). Fe is able to trap both electrons and holes so that photogenerated charge carriers are temporarily separated more effectively (Wang *et al.*, 2003).

$$Fe^{3+} + e^- \rightarrow Fe^{2+}$$

$$Fe^{3+} + h_{vb}^+ \rightarrow Fe^{4+}$$
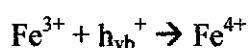
(Ambrus *et al.*, 2008)

From Figure 2.3, it can be seen that the band gap of the TiO$_2$ is lowered after iron doping. Based on energy equation 2.1, the band gap or energy, E, is inversely proportional to the wavelength. When band gap is lowered thus the wavelength increased. Consequently, Fe-doped TiO$_2$ photocatalyst is more active under the visible light.

2.3 Types of Metal-doped TiO$_2$ Photocatalyst

Yoong *et al.* (2009) used Cu-doped TiO$_2$ as a photocatalyst. It was prepared with the dopant metal loading at 2, 5, 10, and 15 wt%.

From Dholam *et al.* (2009), photocatalyts used in the experiment were Cr- and Fe-doped TiO$_2$. Both metal-doped loading were up to a maximum value of 5 wt%. The results obtained indicated higher H$_2$ production rate using Fe/TiO$_2$ (15.5 mmol/h) compared to Cr/TiO$_2$ (5.3 mmol/h). This is because Fe traps both electrons and holes thus avoiding recombination. On the other hand, Cr can only trap one type of charge carrier.

From Navio *et al.* (1998), photocatalyst used in the experiment was Fe-doped TiO$_2$. This experiment used two different precursors to prepare Fe-doped TiO$_2$ photocatalyst which were Fe(NO$_3$)$_3$.9H$_2$O and Fe(III) acetylacetonate, Fe(acac)$_3$. The photocatalysts were tested in two reaction: nitrite oxidation and Cr(VI) reduction.The metal loading was about 0.5 – 5 wt%. The result was catalyst prepared by using Fe(NO$_3$)$_3$.9H$_2$O as a precursor were more efficient for nitrite oxidation than Fe(acac)$_3$ and pure TiO$_2$. For Cr(VI) reduction, both precursors resulted less in efficiency than pure TiO$_2$.

2.4   Methods Used for Catalyst Preparation

Many different methods have previously been reported for metal doping of TiO_2 such as wet impregnation (Litter *et al.*, 1996; Yoong *et al.*, 2009), complex precipitation (Yoong *et al.*, 2009), sol–gel technique (Sonawane *et al.*, 2004; Dholam *et al.*, 2009), and RF-magnetron sputtering (Kitano *et al.*, 2008; Dholam *et al.*, 2009).

From Dholam *et al.* (2009), the samples of catalyst were prepared by sol-gel technique and RF-magnetron sputtering method. Sol-gel technique was used to chemically synthesize metal-doped TiO_2 while RF-magnetron sputtering method physically synthesizes the dopant metal. The results using UV–Visible spectroscopy showed that the sputter-metal-doped-TiO_2 films was much more efficient than the chemically prepared samples to induce red shift of the absorption edge for absorbing visible light. So, from this experiment, RF-magnetron sputtering method is better than sol-gel technique.

From Yoong *et al.* (2009), complex precipitation and wet impregnation method were used for catalysts preparation. The result from this experiment was the photocatalyst with 10 wt% metal dopant at $300^{\circ}C$ calcination temperature prepared by the complex precipitation method showed better activity compared to wet impregnation method. The wet impregnated catalysts did not show any definite trend in the effect of metal loading and calcination temperature on hydrogen production. Only little change in hydrogen production is observed when the copper loading is increased from 2% to 15%.

From Navio *et al.* (1998), wet impregnation method was used for both catalysts preparation by using $Fe(NO_3)_3 \cdot 9H_2O$ and $Fe(acac)_3$ as precursors. There was no comparison method in this experiment as the main objective was to determine the better precursor for the oxidation and reduction process.

Based on Navio *et al.* (1999), Fe-doped TiO_2 was prepared by impregnation of TiO_2 with Fe $(NO_3)_3 \cdot 9H_2O$ and by the sol-gel method using $TiCl_4$ and Fe $(NO_3)_3 \cdot 9H_2O$. It was reported that Fe-doped TiO_2 prepared by the sol-gel method was less active than TiO_2 due to the fact that dopants acted more as recombination centres than a trap sites for charge transfer. It has been observed that at some conditions and for the certain quantity of Fe(III), the dopant can be a center of recombination. Navio *et al.* (1999) proved that the existence of separated hematite or pseudobrookite (Fe_2TiO_5) phases in samples containing more than 2% iron could decrease the activity. It has been also proved that the excess of deposited iron on TiO_2 can form $Fe(OH)^{2+}$, which has the greater adsorption to the incidence light than TiO_2 in the range of 290–400 nm, and can cause decreasing of the Fe-doped TiO_2 photoactivity (Litter *et al.*, 1996). The low calcination temperature, such as 300°C in Fe/TiO_2 preparation appeared to be favoured taking into account its photoactivity (Beata Tryba, 2008).

Nahar *et al.* (2007) stated that Fe-doped TiO_2 photocatalyst could be prepared from Ti element and TiO_2 (P25) particles by using calcinations and impregnation method, respectively. Calcined samples contain only anatase phase, whereas impregnated samples contain anatase and rutile phases for the starting materials P25 (TiO_2). The Fe^{3+} ions caused a higher visible light absorption in calcined samples, whereas in the impregnation method, the same Fe^{3+} cation did very little help in visible light absorption. Fe doping increases the UV and visible light activity for calcined catalyst. However, in the doped samples, the visible activity showed an increase and the UV activity showed a decrease compared with the undoped samples synthesized using the impregnation doping method.

CHAPTER 3

METHODOLOGY

3.1. Experiment Materials

Materials in term of chemicals and apparatus required for the photocatalyst preparation are listed in Table 3.1 and Table 3.2.

Table 3.1: Chemicals required for experiment

	Chemical	Brand name	Purity
1	Glycerol	System	95%
2	Ferric Nitrate, $Fe(NO_3)_3.9H_2O$	Acros	>98%
3	Titanium Oxide, TiO_2	Degussa P25	80% anatase; 20% rutile
4	Sodium Carbonate, Na_2CO_3	Merck	95%

Table 3.2: Apparatus required for experiment

	Apparatus	Model
1	Thermal Gravimetric Analyzer (TGA)	Perkin Elmer
2	Diffuse Reflectance UV-Vis (DR-UV-Vis) spectrometer	Shimadzu 3150
3	Field Emission Scanning Electron Microscope (FESEM)	LEO
4	Fourier Transform Infra-Red (FTIR) spectrometer	Shimadzu
5	X-ray Diffractometer (XRD)	BRUKER D8 AXS
6	Multiport Photocatalytic Reactor	Custom made
7	500 W halogen lamp	
8	Furnace	STRUART
9	Oven	CARBOLITE

3.2 Catalyst Preparation and Pretreatment

Photocatalyst activity is dependent on preparation method and the amount of the metal doped onto TiO_2 (Beata Tryba, 2008). The photocatalyst is prepared by using precipitation with the dopant metal loading of Fe at 0.1, 0.5 and 1.0 wt%. The Fe precursor used is ferric nitrate, $Fe(NO_3)_3.9H_2O$ while glycerol is added to Fe precursor to form a solution. For the precipitation of Fe onto TiO_2, sodium carbonate, Na_2CO_3 is used as the precipitating agent.

Glycerol is added to an aqueous solution of $Fe(NO_3)_3.9H_2O$ (Fe:glycerol mol ratio=1:2). Then, TiO_2 is added to this solution with continuous stirring to form a suspension. Next, with constant stirring, Fe–glycerol solution is precipitated onto TiO_2 particles by adding Na_2CO_3 (0.25 M) dropwise into the suspension. After the precipitate is formed, it is further stirred intensely for 30 min prior to filtering. The precipitate is dried overnight at $70^{o}C$.

Thermal gravimetric analysis is conducted on the raw photocatalyst to estimate the calcinations temperature. Based on the thermogram of the raw photocatalyst from previous article, three calcinations temperature are selected; $300^{o}C$, $400^{o}C$ and $500^{o}C$ for 1 hour. A catalyst sample is given a specific notation as mFe_a, where m is the percentage of Fe loading; Fe refers Fe/TiO_2 photocatalyst and a is the calcination temperature ($x100^{o}C$). Notation for the photocatalysts prepared and process flow for catalyst preparation and pretreatment are shown in Table 3.3 and Figure 3.1. The accuracy of measurement of mass is up to 0.01 mg and for the temperature is $\pm1^{o}C$.

Table 3.3: Notation for the photocatalysts prepared

Fe loading (wt%)	Calcination temperature (^{o}C)		
	300	400	500
0.1	0.1Fe_3	0.1Fe_4	0.1Fe_5
0.5	0.5Fe_3	0.5Fe_40	0.5Fe_5
1.0	1.0Fe_3	1.0Fe_4	1.0Fe_5
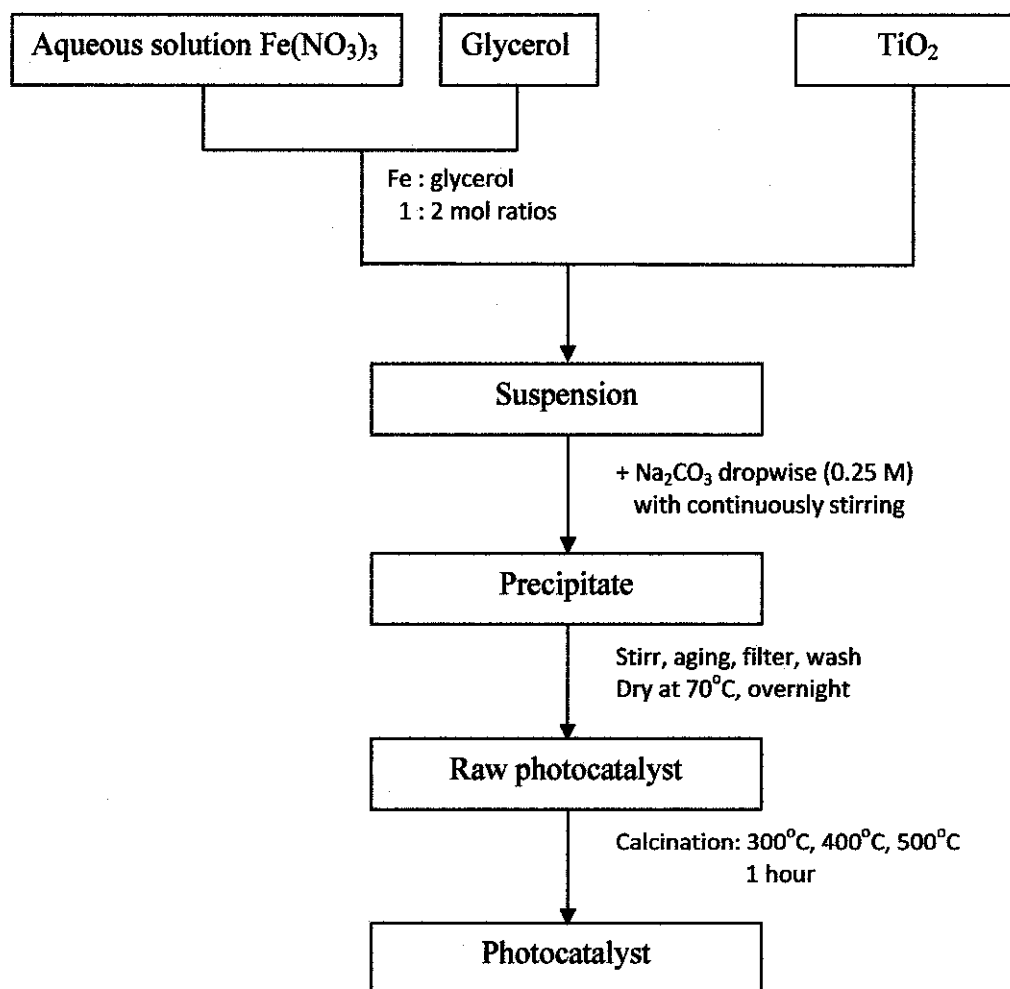
Figure 3.1: Process flow for catalyst preparation and pretreatment

3.3   Catalyst Characterization

Thermal Gravimetric Analysis (TGA)

TGA is used to determine the approximate decomposition temperature of iron in the fresh photocatalyst. The dried photocatalyst is weighed in the range of 5-10 mg using a built-in microbalance attached in the instrument which automatically read the weight of the sample. The rate of heating is maintained at 20 °C/min, and the temperature measurement is carried out from 30 °C to 800 °C with air flowing at 20 mL/min. TGA results is reported as thermograms, plots of the percentage decomposition of the catalyst versus temperature. The decomposition temperature is determined from the plot.

Diffuse Reflectance Spectroscopy (DR- UV-Vis)

Diffuse Reflectance UV-Vis spectra are used to determine whether the band gap of TiO_2 has indeed been reduced by doping with iron. The samples were recorded from the instrument and using Ba_2SO_4 powder as a reference. The powder was filled in a void of sample holder and the surface was smoothened. The layer has to be thick enough and concord with the sample holder surface that all incident light is absorbed or scattered before reaching the back surface of the sample. Typically, a thickness of 1-3 mm is required (Yoong *et al.*, 2009). Reflectance spectra were collected as R= Rsample/Rreference. The graph of remission function, $F(R) = (1-R)^2/2R$ (based on the Kubelka-Munk theory) and energy band gap is plotted. The band gaps of the photocatalysts are obtained as an intercept of the graph.

Fourier Transform Infra-Red (FTIR) Spectroscopy

FTIR spectra are useful for the determination of the functional groups (such as CH_3-, NO_3^-, $-OH$, $C-O$, etc.) present in the catalysts before and after calcinations process. The functional groups are identified by characteristic peaks on the spectrum. The samples were scanned from 4000 cm^{-1} to 400 cm^{-1} by Perkin Elmer Spectrophotometer. 2% amount of each sample was grained with 100% amount of IR-grade KBr and was pressed into a pellet using a hydraulic hand press. Then, the pellet was placed in a sample holder and scanned using the instrument.

X-ray Diffraction (XRD)

X-ray diffraction identifies the type of metal species and also the TiO_2 phases present in the catalyst. The XRD peaks are compared with standards in order to determine the species present in a sample. An adequate amount of powder sample was even-out on a disc using a glass slide and was placed on the stage for scanning. It is conducted with CuK α radiation (40 kV, 40 mA) at 2θ angles from $2°$ to $80°$ with scan speed of $4°$ /min.

Field Emission Scanning Electron Microscopy (FESEM)

The morphologies of the catalysts are determined by using FESEM. FESEM is used because of the higher resolution compared to SEM. An FE-SEM picture is expected to show how well the dopant material is dispersed on the base material, TiO_2, in a catalyst sample. The sample is placed on the stud and coated with a layer of platinum–palladium. Then, the stud with the sample is placed into the instrument for scanning with setting of:

EHT: 5 kV

Working distance, WD: 3.0 - 3.5 mm

Magnification: 100 KX

16

3.4   Photocatalytic Activity

A 500-W halogen lamp is used as a light source simulating solar radiation. It is positioned 15 cm above the multiport reactor. Each of the photocatalyst samples are dispersed in 8 mL of distilled water. The multiport reactor has four ports so that four samples can be tested simultaneously. The gas obtained from the photocatalytic activitiy will be collected in a vertical cylinder over a period of 2 hours (10 minutes per reading) by water displacement. The bubble come out from the tube that is connected to the cylinder with water indicates the present of H_2. The readings of H_2 evolved are taken from the cylinder. Overall reaction is performed at room temperature (about 25 °C).
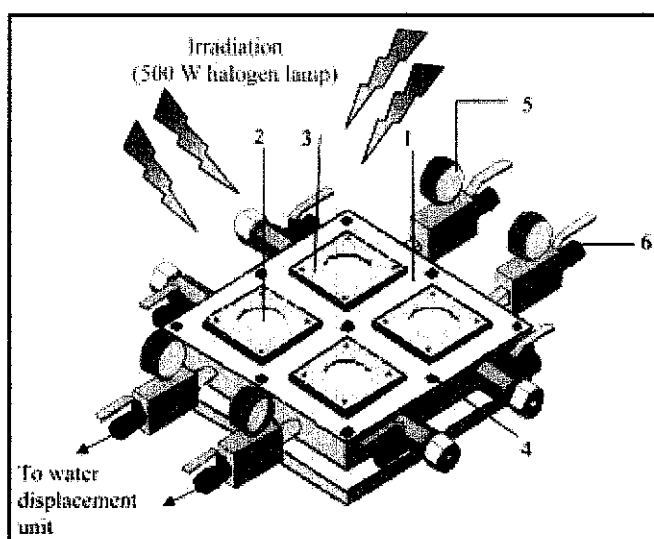
1) Acrylic block	2) Quartz disk	3) Square metal plate
4) Screw	5) Pressure gauge	6) One way valve

Figure 3.2: Multiport Photo Reactor

Figure 3.2 shows the multiport photo reactor; equipment used for studying the photocatalytic reaction. It is made of a thick acrylic block (1) that consist of four reactor ports 40 mL volume each. Each reactor port is covered with a quartz disk (2) held in place by a screwed square metal plate (3) open at the center. The screws (4) used to fix the acrylic block to a base plate. The multi photo reactor is also fitted with pressure gauges (5) and one- way valves (6).

17

3.5   Overall Project Activities

The project begins with research work based on article, journal and books regarding literature review and the concept of the analytical work as references throughout the project. Most of the project progressions are all about experimental works and the concept behind it. The project flows are as follows:
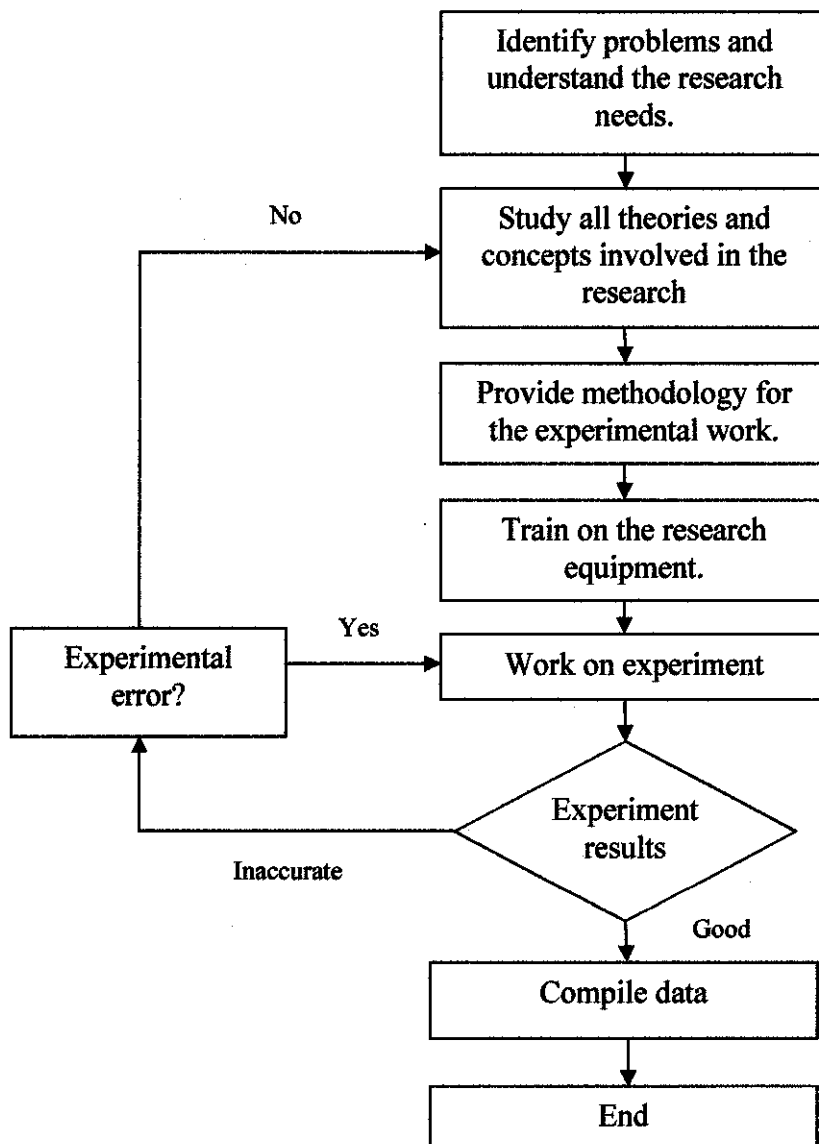

Figure 3.3: Overall project activities

CHAPTER 4

RESULTS AND DISCUSSION

4.1 Photocatalyst Preparation and Pretreatment

The photocatalyst samples prepared by using precipitation method were observed for the physical properties. All samples give colour of brown due to the precursor used was $Fe(NO_3)_3$. The colours of photocatalyst with higher metal loading are darker compared to the lower ones. After drying, the photocatalyst undergo pretreatment process that included calcination temperature and calcination duration time. The optimum calcination temperatures of photocatalyst were determined from the thermal gravimetric analysis (TGA). It was conducted to find at which temperature the photocatalyst start to decompose and the temperature range of the photocatalyst to achieve thermal stability. For this experiment, different calcination temperatures were used ($300^{o}C$, $400^{o}C$, $500^{o}C$) with similar duration for calcination (one hour). After calcination, the photocatalyst samples became smoother and the colour darker compared to the samples before calcination.

4.2 Photocatalytic Activity- Hydrogen Production

In photocatalytic activity to produce H_2, the factors that took into consideration were in term of metal loading and calcination temperature. H_2 evolved was measured experimentally as shown in Figure 4.1. For each experiment of photocatalyst sample, the readings of H_2 evolved were taken for several values according to the availability of the port at the multiport reactor. The final amount of H_2 produced was taken as an average value. Table 4.1 showed the amount of H_2 produced during the photocatalytic reaction for each photocatalyst.

19
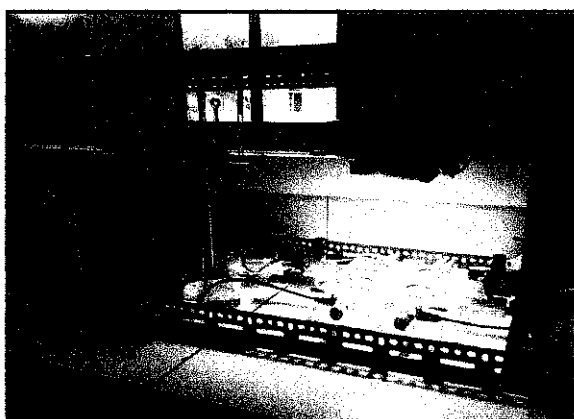
Figure 4.1: Experiment of photocatalytic reaction

Table 4.1: Hydrogen evolution

Photocatalysts	H₂ evolution, ml/h
Pure TiO₂	2.5
0.1Fe_3	4.45
0.5Fe_3	4.30
1.0Fe_3	5.15
0.1Fe_4	4.35
0.5Fe_4	4.90
1.0Fe_4	5.20
0.1Fe_5	4.20
0.5Fe_5	5.10
1.0Fe_5	6.90

Figure 4.2 indicated the result of H_2 produced after 2 hours of reaction for all samples. The only selected photocatalysts based on the good performance in the reaction were sent for characterization to determine their properties. From Figure 4.2, the highest Fe loading (1.0 wt%) gave the highest amount of H_2 being produced for all calcination temperature. For overall reaction, photocatalyst calcined at 500°C displayed better catalytic performance compared to 300°C and 400°C. The best photocatalyst that gave the highest hydrogen production was 1.0Fe_5, about 6.9 ml/h.
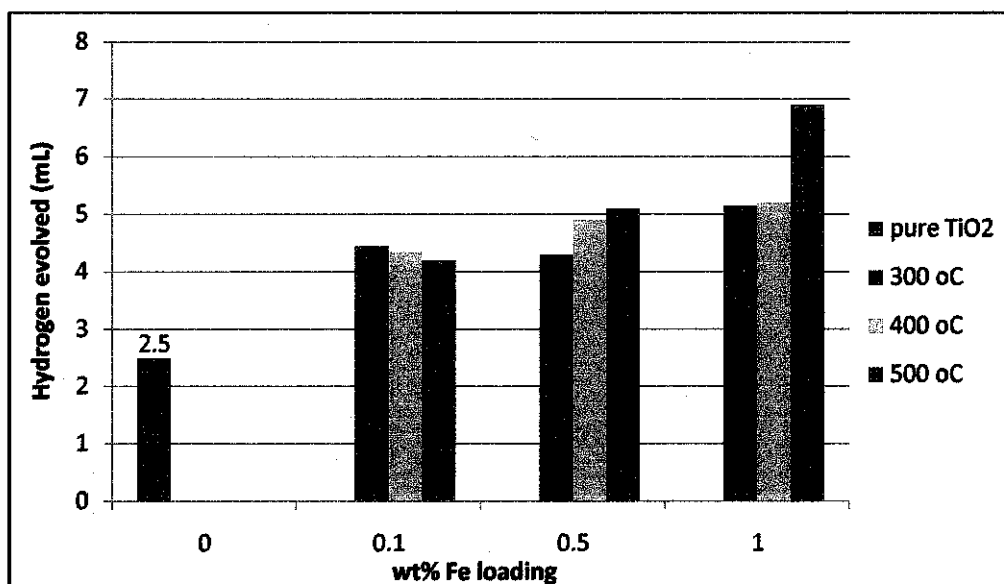
Figure 4.2: Comparison of Fe/TiO$_2$ photocatalyst activity with various calcination temperatures and Fe loading

The increase of Fe loading enhanced the photocatalytic activity by effectively inhibits the electron-hole recombination in TiO$_2$. H$_2$ yield increased with increasing Fe content of the catalyst. According to Wang *et al.* (2001), the formation of surface defects in Fe-doped TiO$_2$ affects the high-photocatalytic activity. When the Fe content increase in the Fe-doped TiO$_2$, the surface defect increased thus led to the high activity compared to pure TiO$_2$.

In term of calcination temperature, the best performance of photocatalyst was at the highest temperature tested that was 500°C. Based on Beata Tryba (2008), at temperature below 400°C, the concentration of titanium defects remained almost constant but decrease as the calcination temperature higher than 600°C due to decrease of the hydroxyls in the crystalline structure thus reduce the photocatalytic activity. Below 400°C, the samples had some brookite and a majority of anatase phase. At the very high calcination temperature, the surface area of the particles was reduced. Sakthivel *et al* (2006) stated that the photocatalytic activity was reduced by decreased in surface area.

4.3   Photocatalyst Characterization

4.3.1   Thermal Gravimetric Analysis (TGA)

TG analysis was applied to study the thermal decomposition behavior of Fe/TiO_2 photocatalyst. The result of thermal decomposition curves of Fe/TiO_2 was shown as thermogram in Figure 4.3. The results contributed an appropriate range of calcination temperature which was used in the further work.

From Figure 4.3, the decomposition curves could be classified into three stages of weight loss. At the first decomposition curve from 26°C to 126°C, the weight loss was 2.6 wt%. It was attributed to the dehydroxylation of water molecule contained or trapped in the sample. The second weight loss of 2.5 wt% from 126°C to 306°C as well as a slight weight loss of 1.3 wt% at the third stage from 306°C to 406°C showed the decomposition of NO_3^- (Wu and Chih, 2001). The total weight loss due to the decomposition was calculated to be 6.4 wt%. A slightly steady horizontal line indicates thermal stability of the photocatalyst and no further weight loss. Moura *et al.* (2005) stated that TG curves were used to obtain information about the optimum calcination temperature of the samples. As a result, for further work, calcination temperature was estimated at 300°C onwards.
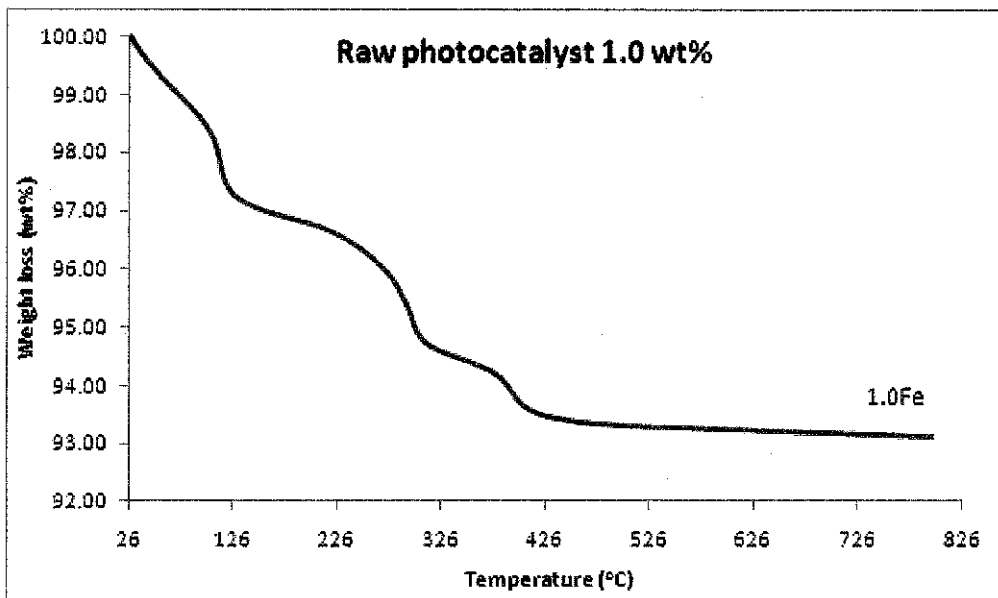
Figure 4.3: Thermal decomposition of 1.0 wt% Fe/TiO$_2$ raw photocatalyst

4.3.2 Diffuse Reflectance UV-Vis (DR-UV-VIS)

UV–vis spectra of all samples were displayed in Figure 4.4. The absorption at wavelength ~380 nm can be assigned to the intrinsic band gap absorption of pure TiO_2. When TiO_2 was doped with Fe, considerable shift of the peak towards the visible range at (>380nm) could be observed for the all sample and the absorption increase with increasing the Fe content, in consistency with the changes in the colour of the samples from white to yellow or light brown (Bahamonde, 2007). The photocatalytic activity of Fe/TiO_2 was promoted with incorporation of Fe ion that shifted the absorption band to the visible range. Thus, it can be deduced that by doping TiO_2 with a transition metal is one of the effective way for visible light response that can play a significant role in enhancing solar hydrogen generation.
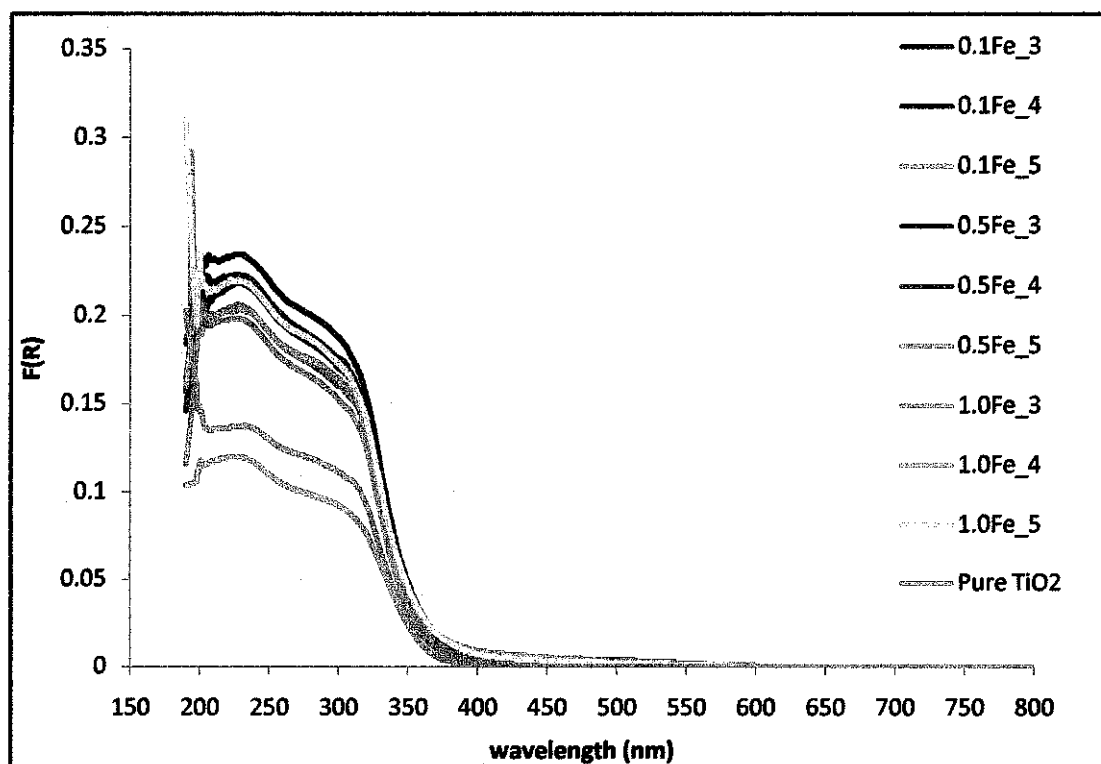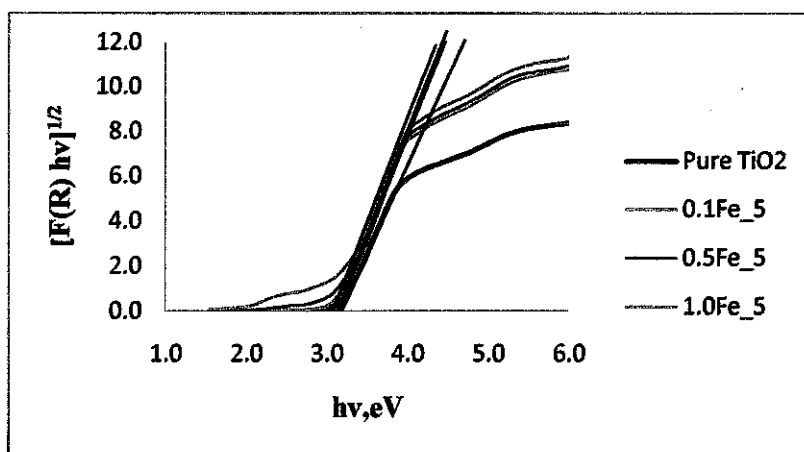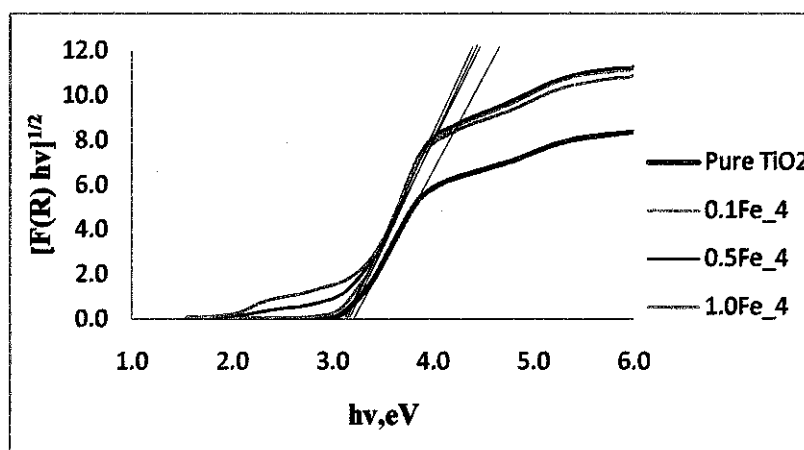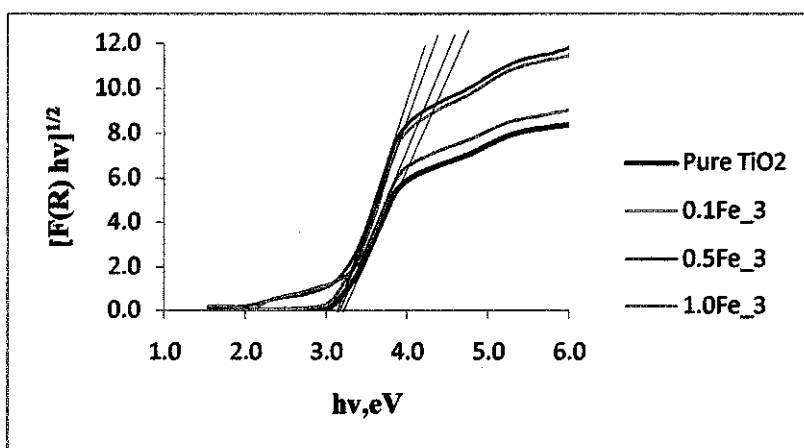

Figure 4.4: DR-UV-Vis spectra of pure TiO_2 and Fe/TiO_2

(a)

(b)

(c)

Figure 4.5: Plot of transformed Kubelka-Munk functions $[F(R).h\nu]^{1/2}$ versus $h\nu$ to estimate band gap energies by linear extrapolation **(a)** $500^{\circ}C$ **(b)** $400^{\circ}C$ and **(c)** $300^{\circ}C$

The Tauc's plot $[F(R).hv]^{1/2}$ vs hv, was used to estimated the band gap calculation for all samples. $F(R) = (1-R)^2/(2R)$ is the formula of Kubelka-Munk and hv is the photon energy (Yuan *et al.*, 2006). By doing extrapolation at photon energy axis, the band gap energies of the photocatalyst samples were determined at the intersection (Figure 4.5). The calculated values of the band gap energy are given in Table 4.2. Refer Appendix C for a sample of band gap calculation by extrapolation.

All the photocatalysts displayed reduction in their band gaps compared to pure TiO_2. The band gap of pure TiO_2 also calculated from Figure 4.5 that gave the value of 3.2eV, same as the theoretical value. From Table 4.2, it was shown that 1.0Fe_5 photocatalyst gave the lowest value of band gap energy, inconformity with the highest hydrogen production from the photocatalytic activity. However, the band gap energy was increased for the other photocatalyst samples. Lowered the band energy will give the longer wavelength thus the photocatalyst be more active under visible light. The red shift of the absorption edge in Fe/TiO_2 might be attributed to the excitation of 3d electrons of Fe^{3+} ion into the TiO_2 conduction band (charge transfer transition) (Bahamonde *et al.*, 2007; Khan *et al.*, 2008)

**Table 4.2:** Band gap energies derived from UV-vis data for the prepared samples compared to pure TiO_2

Photocatalyst	Band gap energy, eV
Pure TiO_2	3.20
0.1Fe_3	3.16
0.5Fe_3	3.15
1.0Fe_3	3.12
0.1Fe_4	3.13
0.5Fe_4	3.10
1.0Fe_4	3.10
0.1Fe_5	3.15
0.5Fe_5	3.11
1.0Fe_5	3.08

### 4.3.3 Fourier Transform Infrared (FTIR)

Figure 4.6 shows the FTIR spectra of Fe/TiO$_2$ photocatalyst with iron loading 1.0 wt% before the calcination and calcination at 500°C for 1 hour. The results for the other photocatalyst samples with different iron loading and calcination temperature are shown in Appendix D.

From Figure 4.6(a), the absorption bands were present at 1383 cm^{-1}, 1408 cm^{-1} and 1470 cm^{-1}. Based on FTIR handbook, Richard et al. (1997), the bands between 1280-1520 cm^{-1} are attributed to the present of nitrate (NO$_3$-) group. Thus, it showed the present of nitrate (NO$_3$-) group in the raw photocatalyst without the calcination. Figure 4.6(b) showed the band at 1383 cm^{-1} that also associated to the present of NO$_3$-. The different is that the band was only one and not very clearly detected compared to the raw photocatalyst. It shows that the calcination temperatures used are sufficient to remove nitrate salt present during the photocatalyst preparation so that the Fe(NO$_3$)$_3$ will not dissolved back into water during the reaction.

This handbook also stated that water of hydration is easily distinguished from hydroxyl group by the present of the H-O-H bending motion which produces a medium band in the region 1600-1650 cm^{-1}. Figures, 4.6(a) and 4.6(b) have the bands at 1630 cm-^{1} and 1616 cm^{-1}, respectively. It showed the present of H-O-H bending for both uncalcine and calcined photocatalysts. The bands between 3200-3700 cm^{-1} were associated with O-H stretching vibrations of water and hydroxyl groups in the photocatalyst. The Ti-O stretching vibrations were detected from the broad bands observed between 400–900 cm^{-1} (Linacero et al., 2006; Porkodi and Arokiamary, 2007).
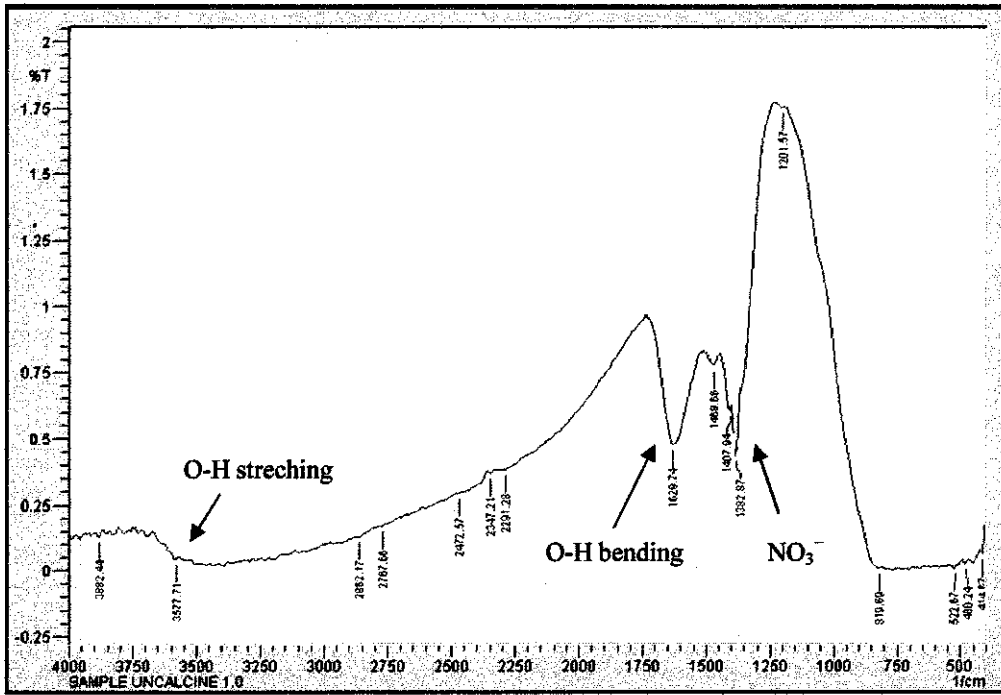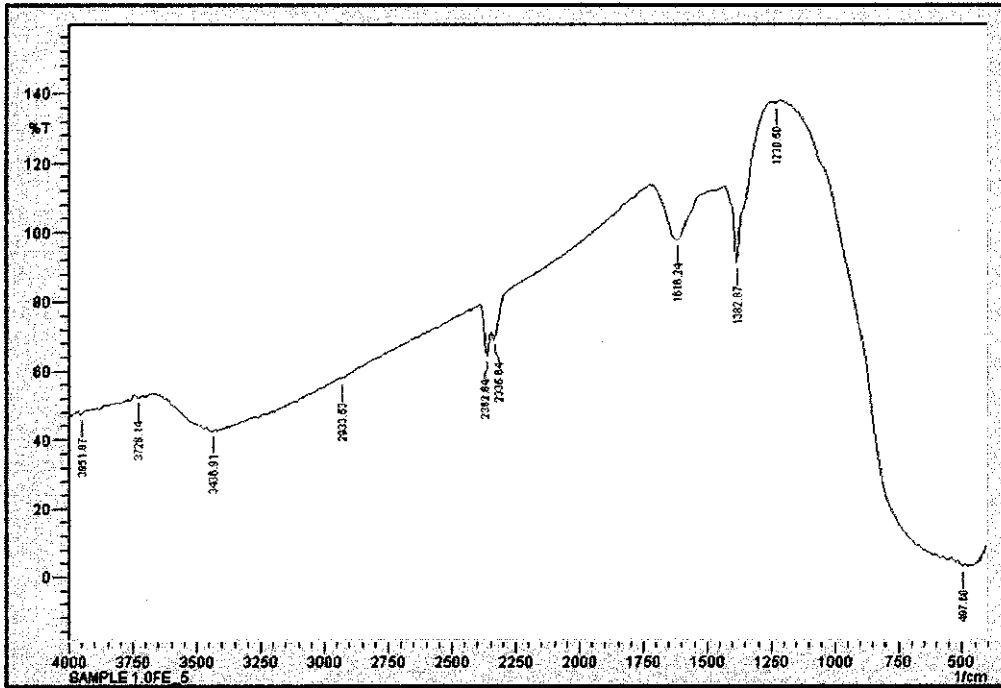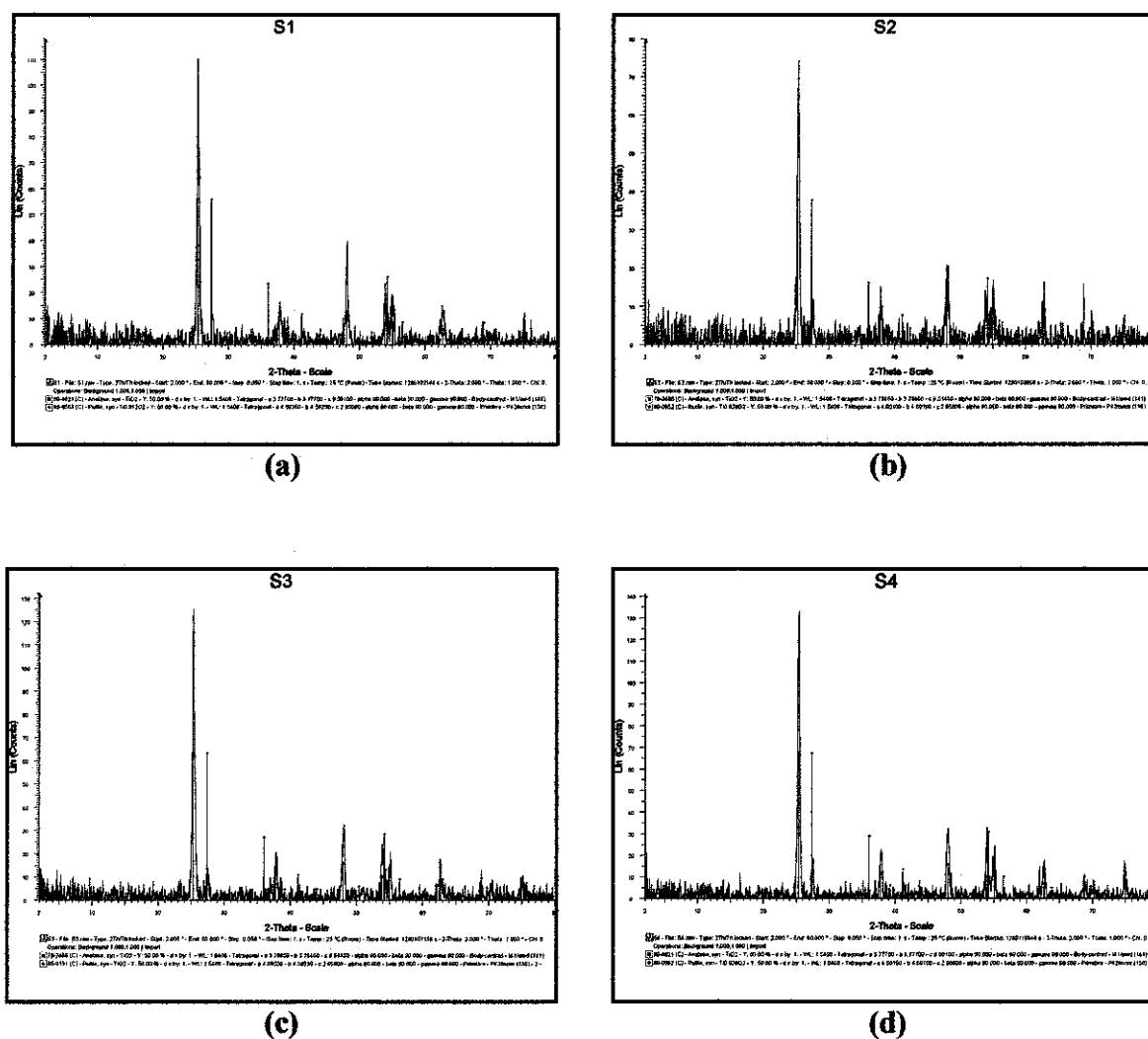
Figure 4.6: FTIR spectra of 1.0 wt% Fe/TiO₂ photocatalyst **(a)** before calcination and **(b)** after calcination at 500°C

4.3.4 X-ray Diffraction (XRD)

Figure 4.7: XRD diffractograms for Fe/TiO$_2$ (a) 0.1Fe_5 (b) 0.5Fe_5 (c) 1.0Fe_5 and
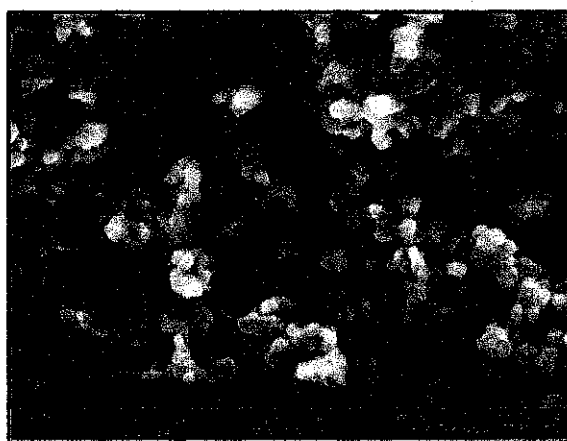
(d) 1.0Fe_4

From Figure 4.7, all diffractograms only show the peaks of anatase and rutile of TiO$_2$ and no peaks of FeO were noticeable even at the higher calcination temperature and higher Fe-loading. This could be due to the high degree of dispersion of FeO species present on the surface of TiO$_2$ without significant changing of the lattice (Yuan *et al.*, 2006).

### 4.3.5 Field Emission Scanning Electron Microscopy (FESEM)

The Fe/TiO$_2$ photocatalyst were tested by using FESEM for the morphology and EDX (Energy Dispersive X-ray). Figure 4.8(a)-(c) show the FESEM images of the photocatalyst. The photocatalyst particles were found spherical in shape and irregularities of the structures were observed. Irregularities happen probably because of the grinding process during the preparation of the samples. There was not much difference between the particles of TiO$_2$ (support) and Fe (metal-doped) in terms of morphology. It showed that during the photocatalyst preparation, the Fe clusters were evenly dispersed or incorporated onto the support. Yoong *et al.* (2009) found that the metal was well-dispersed onto the support using precipitation method while for wet impregnation method, metal agglomeration occurred indicated by the presence of rod like and platelet shape. The sizes of the particles were very small (around 20-100 nm) for all samples. Refer to Appendix E for the morphology of other photocatalyst samples.

From Figure 4.9 and Table 4.3, it can be observed clearly that the element of Fe was present in the photocatalyst. For 1.0wt% iron loading sample, the result of wt% of Fe from 500°C calcination temperature was 0.79 wt%, followed by 0.62 wt% and 0.60 wt% for 400°C and 300°C, respectively. The different of wt% of Fe were due to the different point that the samples were scanned during the test. In the given typical EDX spectra in Figure 4.9, all the expected elements were present including Ti, Fe and O, with additionally Na element that came from the precipitation agent because washing was not done after the filtration during the preparation of photocatalyst and C element from the carbon film used to stick the sample to the stud during the FESEM test.
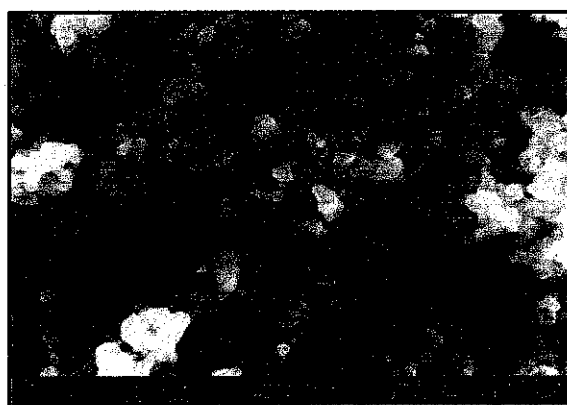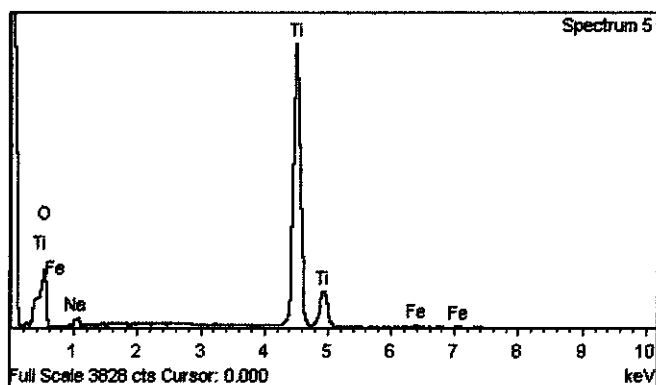
30
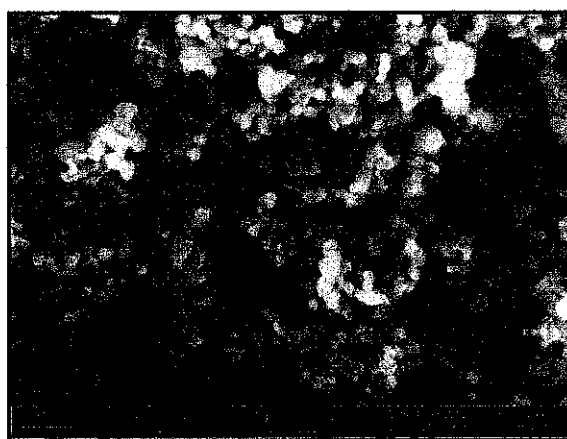
(a) 1.0Fe_5

(b) 1.0Fe_4

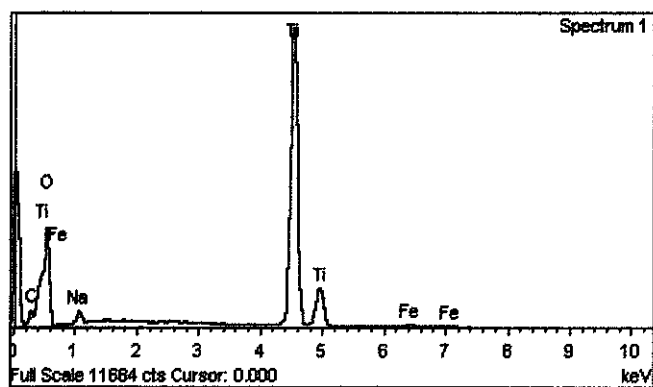(c) 1.0Fe_3

Figure 4.8: The FESEM micrographs of Fe/TiO$_2$

31

(a.1) 1.0Fe_5

Element	Weight%	Atomic%
O K	47.58	72.58
Na K	1.38	1.47
Ti K	50.25	25.60
Fe K	0.79	0.34
Total	100.0	

(a.2) 1.0Fe_5

(b.1) 1.0Fe_4

Element	Weight%	Atomic%
C K	9.48	16.37
O K	50.80	65.84
Na K	1.37	1.23
Ti K	37.73	16.33
Fe K	0.62	0.23
Total	100.00	

(b.2) 1.0Fe_4
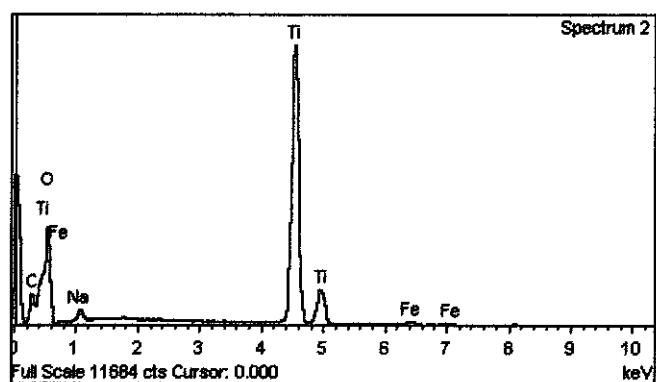
(c.1) 1.0Fe_3

Element	Weight%	Atomic%
C K	4.69	8.50
O K	52.28	71.18
Na K	1.61	1.52
Ti K	40.83	18.57
Fe K	0.60	0.23
Total	100.00	

(c.2) 1.0Fe_3

Figure 4.9 and Table 4.3: EDX spectra of Fe/TiO_2

CHAPTER 5

CONCLUSION AND RECOMMENDATIONS

5.1 Conclusion

From the result obtained in Chapter 4, the efficiency of TiO_2 photocatalyst can be increased by doping with Fe. The absorption edge of the photocatalyst was shifted from UV region to visible region in order to harvest the abundance of solar energy that mainly consists of the visible light for the hydrogen production from water. The estimated band gap was shown in Table 4.2 in which it has been reduced from 3.2 eV to 3.08 eV. The lowered band gap reduction may be due to the presence of FeO crystals incorporated onto TiO_2. The study showed that the incorporation of transition metal tremendously improved the photocatalytic activity compared to TiO_2.

From the study carried out, 1.0wt% Fe/TiO_2 calcined at 500°C at 1h photocatalyst displayed the best performances for photocatalytic activity that produced the highest amount of hydrogen, 6.9 mL compared to others. The good performance is suggested to be contributed by the reducing of band gap of TiO_2 (3.2 eV). In principle, all these properties make the new specimens to be expected to possess a good photocatalytic activity. It is anticipated that the low cost, environmentally friendly photocatalytic activity for hydrogen production will play an important role in the hydrogen production and contribute much to the coming hydrogen economy.

5.2 Recommendations and future work

Future studies of the project are recommended to optimize the photocatalyst especially for the reaction. Some factors need to be manipulated based on the current photocatalyst preparation such as change the precipitation agent (e.g: ammonia), increase the aging time of the precipitate to make sure all the particles are well accumulate and add the reduction process after calcination in pretreatment part to convert FeO to Fe. It is recommended to conduct more characterization for in-depth study of the properties of the photocatalyst such as BET, TEM, TPR and XPS. Besides, the medium for the photocatalytic reaction can be varies to sea water or mixture of distilled water and glycerol instead of current medium that is distilled water to study the best medium for hydrogen production.

REFERENCES

Adan, C., Bahamonde, A., Fernandez-Garcia, M. and Martinez-Arias, A. (2007). Structure and activity of nanosized iron-doped anatase TiO_2 catalysts for phenol photocatalytic degradation, *Applied Catalysis B*, 72, pp 11–17.

Ambrus, Z., Balázs, N., Alapi, T., Wittmann, G., Sipos, P., Dombi, A. (2008). Synthesis, structure and photocatalytic properties of Fe(III)-doped TiO_2 prepared from $TiCl_3$, *Applied Catalysis B: Environmental*, 81, 1-2, pp 27-37.

Amit, S. and Sharma, B. P. (2002). Preparation of copper powder by glycerol process, *Materials Research Bulletin*, 37, pp 407-416.

Beata Tryba. (2008). Increase of the photocatalytic activity of TiO_2 by carbon and iron modifications, *International Journal of Photoenergy*, pp 1-15.

Cong, Y., Zhang, J., Chen, F., Anpo, M. and He, D. (2007). Preparation, photocatalytic activity, and mechanism of nano-TiO_2 Co-doped with nitrogen and iron (III), *The Journal of Physical Chemistry C*, pp 10618-10623.

Craig, A. G., Ooman, K. V., Sudhir, R. (2008). The solar generation of hydrogen by water photoelectrolysis, *Light, Water, Hydrogen*, 7.

Dholam, R., Patel, N., Adami, M., and Miotello, A. (2009). Hydrogen production by photocatalytic water-spltting using Cr- or Fe-doped TiO_2 composite thin films photocatalyst, *International Journal of Hydrogen Energy*, 34, 13, pp 5337-5346.

Fujishima, A., Zhang, X., and Tryk, D. A. (2008). TiO_2 photocatalysis and related surface phenomena, *Surface Science Reports*, 63, 12, pp 515-582.

Green Earth Nano Science Inc. (2006-2008), Mechanism of Photocatalysis, http://www.mchnanosolutions.com/mechanism.html, 5 March 2010.

Herrmann, J. (1999). Heterogeneous photocatalysis: Fundamentals and applications to the removal of various types of aqueous pollutants, *Catalysis Today*, 53, 1, pp 115-129.

Khan, M. A., Woo, S. I., and Yang, O. (2008). Hydrothermally stabilized Fe(III) doped titania active under visible light for water splitting reaction, *International Journal of Hydrogen Energy*, 33, 20, pp 5345-5353.

Kitano, M., Tsujimaru, K., Anpo, M. (2008). Hydrogen production using highly active titanium oxide-based photocatalysts, *Topics in Catalyst*, pp 4-17.

Kitirote, W., Laksana, L., Pongtanawat, K., Nurak, G. and Keisuke, F. (2010). Calcination temperature effect on solvothermal Fe–TiO_2 and its performance under visible light irradiation, *Journal of the Taiwan Institute of Chemical Engineers*, 41, pp 612–616.

Li, Y., Mei, C., Jerry, R., Yide, X. and Wenjie, S. (2006). Glycerol-mediated synthesis of Ni and Ni/NiO core-shell nanoparticle, *Materials Letter*, 60, pp 750-753.

Linacero, R., Aguado-Serrano, J. and Rojas-Cervantes, M. L. (2006). Preparation of mesoporous TiO_2 by the sol-gel method assisted by surfactants, *Journal of Materials Science*, 41, pp 2457-2464.

Litter, M. I., and Navío, J. A. (1996). Photocatalytic properties of iron-doped titania semiconductors, *Journal of Photochemistry and Photobiology A: Chemistry*, 98, 3, pp 171-181.

Milis, A., Peral, J., Domenech, X. and Navio, J. A. (1994). Heterogeneous photocatalytic oxidation of nitrite over iron-doped TiO_2 samples, *Journal of Molecular Catalysis*, 87, pp 67–74.

36

Moura, J. A., Araujo, A. S., Ana, C. S. L. S. C., Joana, M. F. B. A., Silva, A. O. S. and Souza, M. J. B. (2005). Thermal analysis applied to characterization of copper and nickel catalysts, *Journal of Thermal Analysis and Calorimetry*, 79, pp 435-438.

Nahar, M.S., Hasegawa, K., Kagaya, S., Kuroda, S. (2007). Comparative assessment of the efficiency of Fe-doped TiO_2 prepared by two doping methods and photocatalytic degradation of phenol in domestic water suspensions, *Science and Technology of Advanced Materials 8*, pp 286-291.

Navío, J. A., Colón, G., Litter, M. I., Bianco, G. N. (1996). Synthesis, characterization and photocatalytic properties of iron-doped titania semiconductors prepared from TiO_2 and iron(III) acetylacetonate, *Journal of Molecular Catalysis A*, pp 267-276.

Navío, J. A., Colón, G., Trillas, M., Peral, J., Domènech, X., Testa, J. J.(1998). Heterogeneous photocatalytic reactions of nitrite oxidation and cr(VI) reduction on iron-doped titania prepared by the wet impregnation method, *Applied Catalysis B: Environmental*, 16, 2, pp 187-196.

Navio, J. A., Testa, J. J., Djedjeian, P., Padron, J. R., Rodriguez, D. and Litter, M. I. (1999). Iron-doped titania powders prepared by a sol-gel method—part II: photocatalytic properties, *Applied Catalysis A*, 178, pp 191–203.

Ni, M., Leung, M. K. H., Leung, D. Y. C. and Sumathy, K. (2007). A review and recent developments in photocatalytic water-splitting using TiO_2 for hydrogen production, *Renewable and Sustainable Energy Reviews*, 11, 3, pp 401-425.

Pavasupree, S. and Yoshikawa, S. (2007). Synthesis, characterization, photocatalytic activity and dye-sensitized solar cell performance of nanorods/nanoparticles TiO_2, http://www.mrs.org/smrs/bin.asp?CID=7363&DID=182314&DOC=FILE.PDF, 15 March 2010.

Porkodi, K. and Arokiamary, S. D. (2007). Synthesis and spectroscopic characterization of nanostructured anatase Titania: A Photocatalyst, *Materials Characterization*, 58, pp 495-503.

Richard, A. N. and Ronald O.K. (1997). Infrared spectra of inorganic compounds, *Handbook of infrared and raman spectra of inorganic compounds and organic salt*, 4.

Shon, H., Phuntsho, S., Okour, Y., Cho, D.L., Kim, K.S., Li, H.J., Na, S.Y., Kim, J.B., and Kim, J.H. (2008). Visible Light Responsive Titanium Dioxide (TiO_2), *J. Korean Ind. Eng. Chem.*, pp 1-16.

S. W. Bae, P. H. Borse, S. J. Hong, S. J. Jang, J. S. Lee. (2007). Photophysical properties of nanosized metal-doped TiO_2 photocatalyst working under visible light, *Journal of Korean Physical Society*, 51, pp S22-S26.

Titaniumart.com. (2003), Photocatalysis Applications of Titanium Dioxide TiO_2, http://www.titaniumart.com/photocatalysis-ti02.html, 5 March 2010.

Tong, T., Zhang, J., Tian, B., Chen, F. and He, D. (2008). Preparation of Fe^{3+}-doped TiO_2 catalysts by controlled hydrolysis of titanium alkoxide and study on their photocatalytic activity for methyl orange degradation, *Journal of Hazardous Materials*, 155, 3, pp 572-579.

Wang, C., Bottcher, C., Bahnemann, D.W. and Dohrmann, J. K. (2003). A comparative study of nanometer sized Fe(III)-doped TiO_2 photocatalysts: synthesis, characterization and activity, *Journal of Materials Chemistry*, 13, pp 2322–2329.

Wang, J., A., Limas-Ballesteros, R., Lopez, T., et al. (2001). Quantitative determination of titanium lattice defects and solid-stated reaction mechanism in iron-doped TiO_2 photocatalyst, *Journal of Physical Chemistry B*, 105, 40, pp 9692-9698.

Wu, J. C. S. and Chih, Y. Y. (2001). Sol-gel-derived photosensitive TiO_2 and Cu/TiO_2 using homogeneous hydrolysis technique, *Journal of Materials Resources*, 16, pp 615-620.

Yoong, L. S., Chong, F. K. and Dutta, B. K. (2009). Development of copper-doped TiO_2 photocatalyst for hydrogen production under visible light, *Energy*, 34, 10, pp 1652-1661.

Yuan, Z., Wang, Y., Sun., Y., Wang, J. and Bie, L. (2006). Sunlight-activated $AlFeO_3/TiO_2$ photocatalys, *Science in China: Series B Chemistry*, 49, pp 67-74.

APPENDIX A

Catalyst Preparation

Table A.1: Molecular Weight for chemicals involves in catalyst preparation

Chemicals	Molecular Formula	Molecular Weight (g/mol)
Ferric Nitrate	$Fe(NO_3)_3.9H_2O$	404.00
Iron Metal	Fe	55.85
Titanium Dioxide	TiO_2	79.87
Glycerol	$C_3H_5(OH)_3$	92.094

Table A.2: Summary of mass for respective loading

Content	Fe (III) loading (wt%)		
	0.1	0.5	1.0
Amount of catalyst (g)	20	20	20
Mass of Fe (g)	0.02	0.1	0.2
Mass of TiO_2 (g)	19.98	19.9	19.8
Mass of $Fe(NO_3)_3.9H_2O$ (g)	0.1447	0.7234	1.4467
Volume of glycerol, 95% purity (ml)	0.0523	0.2617	0.5235
10% purity (ml)	0.50	2.49	4.97

I

Sample of calculation of Fe (0.1wt%)

Basis: 20g of catalyst

For   100g catalyst → 0.1g of Fe metal

        20g of catalyst → x

So,

$$x = \frac{20g \text{ of catalyst}}{100g \text{ of catalyst}} \times 0.1g \text{ of Fe metal}$$

$$= 0.02 \text{ g of Fe metal}$$

Hence, 1 mol of $Fe(NO_3)_3.9H_2O$ → 55.85g of Fe

        Y mol of Fe $Fe(NO_3)_3.9H_2O$ → 0.02g of Fe

$$Y = \frac{0.02g \text{ of Fe}}{55.85g \text{ of Fe}} \times 1 \text{ mol of Fe(NO3)3.9H2O}$$

$$= 0.0003581021 \text{ mol of } Fe(NO_3)_3.9H_2O$$

The amount of $Fe(NO_3)_3.9H_2O$ is:

        1 mol of $Fe(NO_3)_3.9H_2O$ → 404g/mol

        0.000358102 mol of $Fe(NO_3)_3.9H_2O$ → Z

$$Z = \frac{0.000358102 \text{ mol of Fe(NO3)3.9H2O}}{1 \text{ mol of Fe(NO3)3.9H2O}} \times 404g/mol$$

$$= 0.1447g \text{ of } Fe(NO_3)_3.9H_2O$$

Sample of calculation of glycerol (0.1wt%)

Note that;

        Glycerol: $Fe(NO_3)_3.9H_2O$ = 2:1

        2 mol of glycerol = 1 mol of $Fe(NO_3)_3.9H_2O$

        A mol of glycerol = 0.000358102 mol of $Fe(NO_3).9H_2O$

$$A = \frac{0.000358102 \text{ mol of Fe(NO3).9H2O}}{1 \text{ mol of Fe(NO3).9H2O}} \times 2 \text{ mol of glycerol}$$

$$= 0.000716204 \text{ mol of glycerol}$$

The amount of glycerol is:

1 mol of glycerol $\rightarrow$ 92.094g of glycerol

0.0007162042 mol of glycerol $\rightarrow$ B

$$B = \frac{0.0007162042 \text{ mol of glycerol}}{1 \text{ mol of glycerol}} \times 92.094 \text{g of glycerol}$$

$$= 0.065958109 \text{g of glycerol}$$

Density of glycerol = 1.26 g/ml

$$\text{Volume of glycerol (ml)} = \frac{\text{Mass of glycerol (g)}}{\text{Density of glycerol } (\frac{g}{ml})}$$

$$= \frac{1g}{1.26 g/ml}$$

$$= 0.79365 \text{ ml}$$

So,

1 g of glycerol $\rightarrow$ 0.79365 ml of glycerol

0.065958109g of glycerol $\rightarrow$ C ml of glycerol

$$C = \frac{0.065958109 \text{g of glycerol}}{1 \text{ g of glycerol}} \times 0.79365 \text{ ml of glycerol}$$

$$= 0.0523 \text{ ml of glycerol}$$

Dilution of glycerol:

95% purity $\rightarrow$ D

10%purity $\rightarrow$ 100ml

Amount of glycerol to be diluted, D = 10.53 ml

Amount to be used = (100/10.53) x 0.0523

$$= 0.50 \text{ ml}$$

APPENDIX B

Sample of calculation and Preparation of 0.25M Na₂CO₃

a) Na_2CO_3 Mass Calculation

MW of Na_2CO_3 = 105.99 g/mol

$$\text{Numbers of mol (mol)} = \frac{\text{mass (g)}}{\text{MW} \left(\frac{g}{mol}\right)}$$

(Eq: B.a1)

$$\text{Molarity} = \frac{\text{Numbers of mol (mol)}}{\text{Volume (L)}}$$

(Eq: B.a2)

Substitute (Eq. B.a1) into (Eq: B.a2):

$$\text{Molarity} = \frac{\text{Mass (g)}/\text{MW} \left(\frac{g}{mol}\right)}{\text{Volume (L)}}$$

So,

$$\text{Mass (g)} = \text{Molarity (M)} \times \text{MW} \left(\frac{g}{mol}\right) \times \text{Volume (L)}$$

$$\text{Mass (g)} = 0.25 \text{ M} \times \frac{105.99g}{mol} \times 1L$$

$$= 26.498 \text{ g of } Na_2CO_3$$

b) Preparation of 1L Na_2CO_3 Solution

1) 26.498g of Na_2CO_3 palettes were measured using the electronic weighing scale.

2) Then, the palettes were transferred into 500 ml beaker and diluted with distilled water.

3) The diluted solution was poured into 1000 ml volumetric flask, and distilled water was added slowly until the solution reaches the marker.

APPENDIX C

[Band Gap Estimation from DR-UV-Vis Spectra Results]
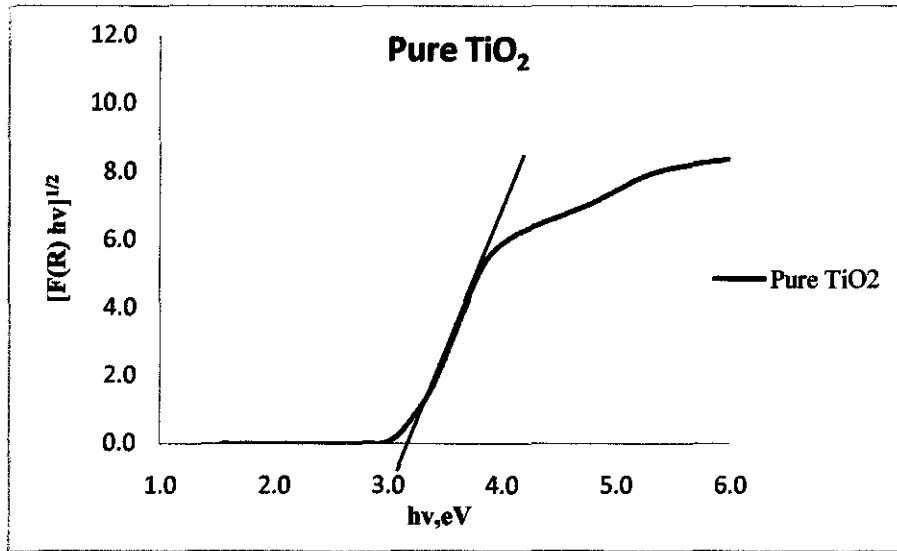
Figure C.1: DR-UV-Vis spectra for TiO_2

The band gap for TiO_2 is determined from the extrapolation of the absorption edge onto the energy axis (Eg) using the linear equation, $y = mx + c$.

Two plots were obtained from the linear curve of TiO_2; (3.3, 0.8) and (4.0, 6.6)

$m = (y_1-y_2)/(x_1-x_2)$

$\quad = (6.6-0.8)/(4.0-3.3)$

$\quad = 8.2857$

Put point (4.0, 6.6) into $y = mx + c$

$$6.6 = 8.2857(4.0) + c$$

Therefore, $c = -26.5428$

$y = 8.2857x - 26.5428$

When $y = 0$, $x = 3.20$

Therefore the estimated band gap for TiO2 is 3.20.

APPENDIX D

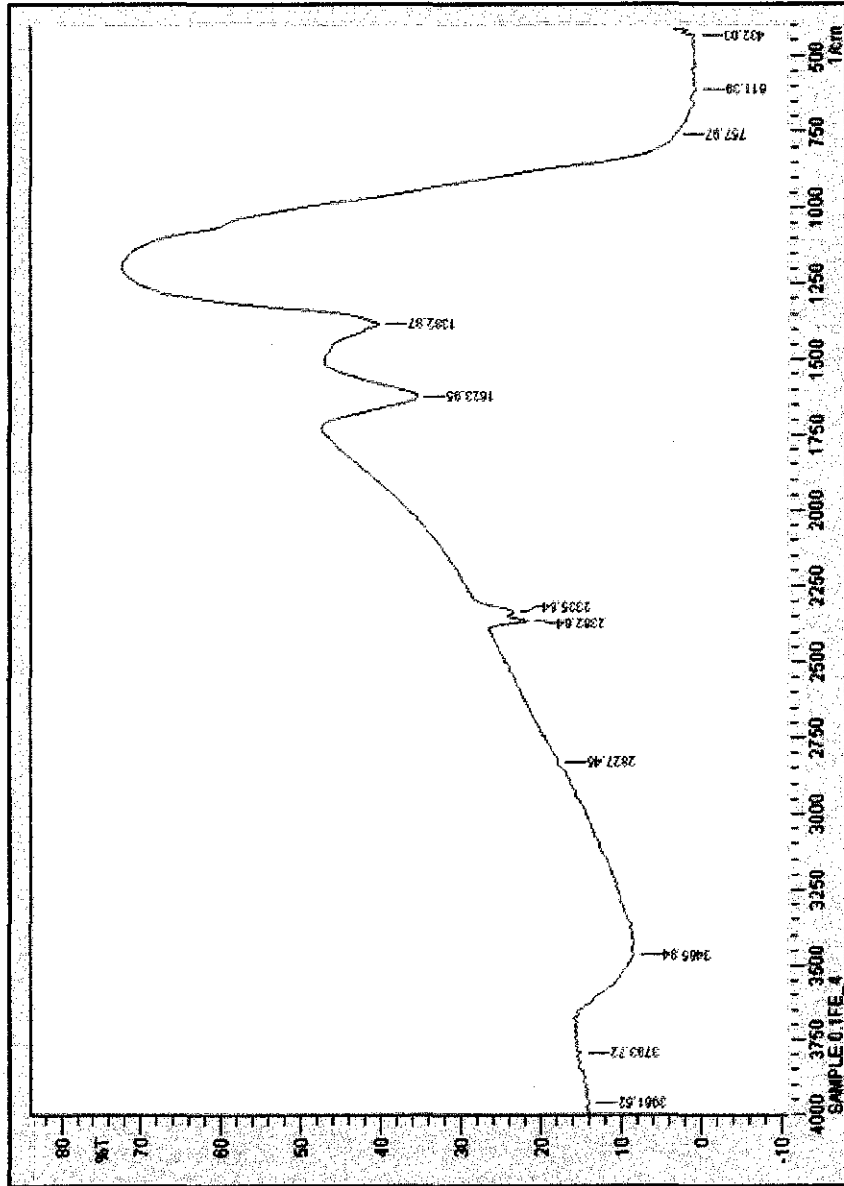## Fresh photocatalyst 0.1 wt% (0.1Fe)
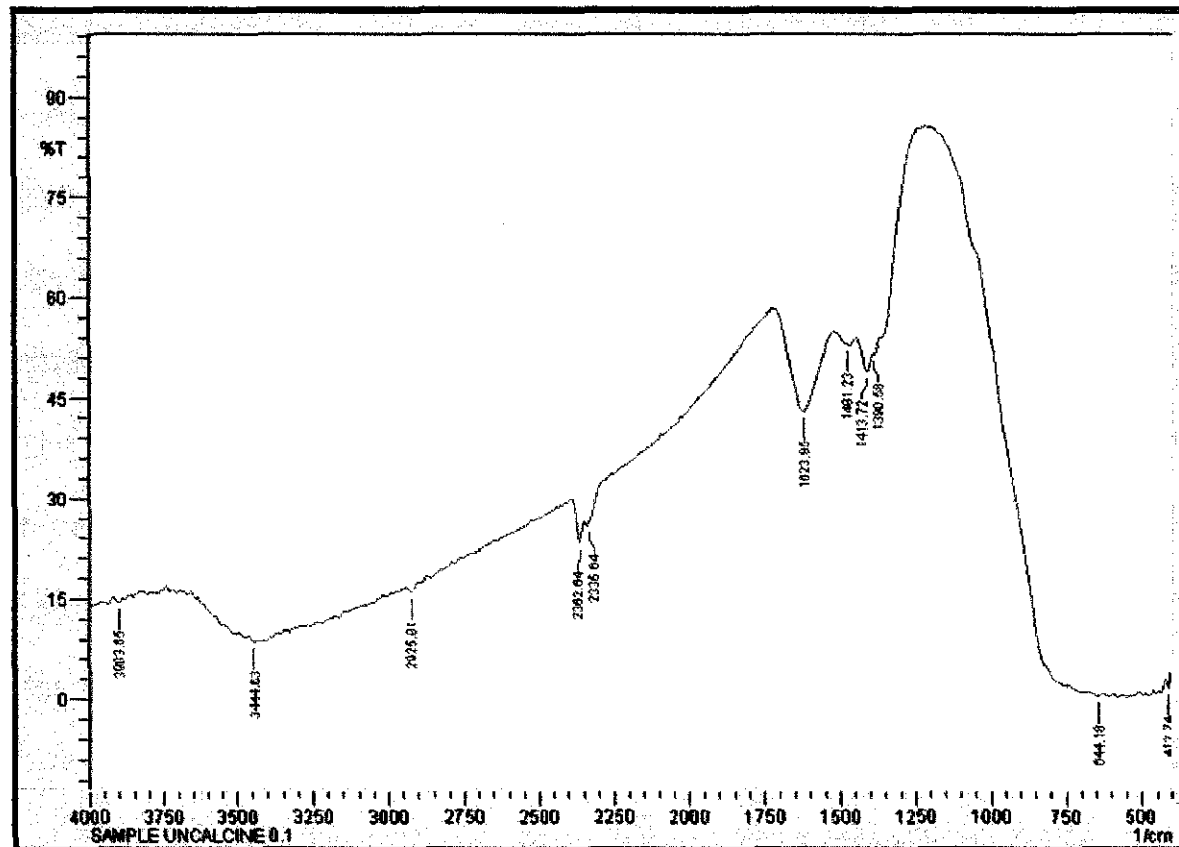
Fresh photocatalyst 0.5 wt% (0.5Fe)

0.1Fe_3

VIII
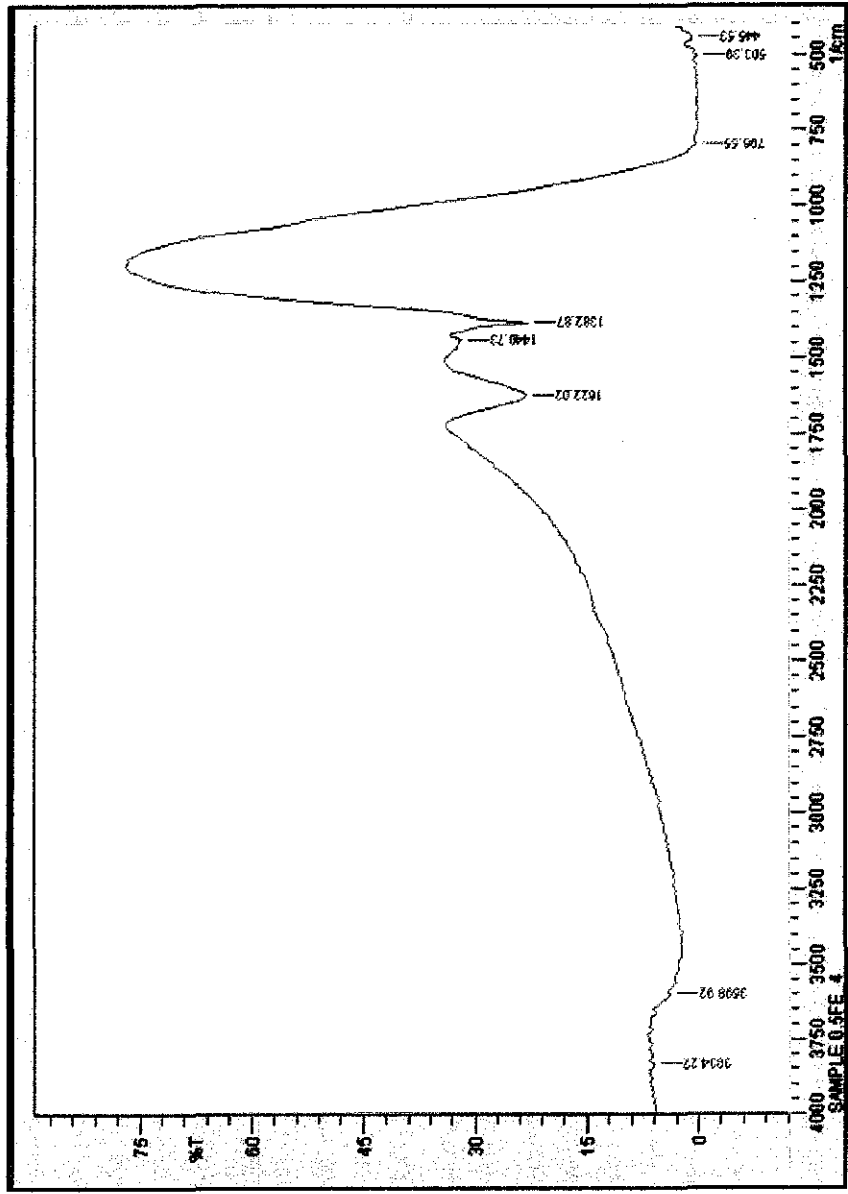
0.5Fe_3

IX

1.0Fe_3

0.1Fe_4

XI

SAMPLE 0.1FE_4

0.5Fe_4

XII

1.0Fe_4

XIII

0.1Fe_5

XIV

0.5Fe_5

XV

APPENDIX E

0.5Fe_5

0.5Fe_4

0.5Fe_3

0.1Fe_5

0.1Fe_4

0.1Fe_3